Chaos, Solitons and Fractals 210 (2026) 118675

Contents lists available at ScienceDirect

Chaos, Solitons and Fractals

journal homepage: www.elsevier.com/locate/chaos

Multiscale integration of pairwise and higher-order fMRI-based functional connectivity in hypergraph neural networks enhances autism spectrum disorder classification ☆

Elena N. Pitsik [a], Semen A. Kurkin [a], Alexander E. Hramov [a,b,*]

[a] Research Institute for Applied Artificial Intelligence and Digital Solutions, Plekhanov Russian University of Economics, 36 Stremyanny Lane, Moscow, 115054, Russia

[b] Pirogov National Medical and Surgical Center, 70 Nizhnyaya Pervomayskaya str., Moscow, 105203, Russia

ARTICLE INFO

Keywords:
Hypergraph neural network
Higher-order interactions
fMRI connectivity
Functional brain network

ABSTRACT

Conventional graph-based analyses of functional brain networks capture only pairwise interactions, overlooking higher-order polyadic dependencies that are increasingly recognized as fundamental to brain computation. Here we apply hypergraph neural networks (HGNNs) to resting-state fMRI data from the ABIDE dataset (408 ASD, 476 typically developing subjects; AAL atlas, 116 ROIs) and demonstrate that the synergistic integration of higher-order hypergraph structure with pairwise functional connectivity features is essential for accurate autism spectrum disorder (ASD) classification. Hypergraph representations are constructed via sparse group lasso, and two UniGNN variants (UniGCN and UniGIN) are benchmarked against SVM and standard GCN baselines. UniGIN with pairwise connectivity profiles as node features achieves the best performance (F1 = 0.77, AUC = 0.80, balanced accuracy = 0.76), substantially outperforming the same architecture with time-series-derived features (F1 = 0.64, AUC = 0.74) and all pairwise-only models. This result establishes that neither hypergraph topology alone nor pairwise connectivity alone suffices: the hypergraph defines meso-scale modular structure while pairwise features encode fine-grained dyadic interactions, and both scales are needed for optimal discrimination. Consensus network analysis reveals that group-level differences are structured and systematic at the hypergraph level but region-specific at the pairwise level. Contrastive comparison of consensus hypergraphs shows that 9 of 10 hyperedges are topologically identical between ASD and TD groups, sharing a conserved triple-network (DMN–CEN–SN) backbone. The primary divergence involves the cerebellum: ASD exhibits a decoupling of visual–cerebellar coordination, the emergence of an isolated cerebellar module with expanded Vermis recruitment, and an aberrant fronto-cerebellar hyperedge absent in controls. These findings provide a multi-scale framework for understanding ASD-related brain network alterations and establish a methodological principle that advancing beyond pairwise interactions requires integrating, not replacing, dyadic analysis within higher-order topological representations.

☆ This article is part of a Special issue entitled: 'Tribute to Stefano Boccaletti' published in Chaos, Solitons and Fractals.

* Corresponding author at: Research Institute for Applied Artificial Intelligence and Digital Solutions, Plekhanov Russian University of Economics, 36 Stremyanny Lane, Moscow, 115054, Russia.

E-mail address: hramovae@gmail.com (A.E. Hramov).

https://doi.org/10.1016/j.chaos.2026.118675
Received 4 April 2026; Received in revised form 18 May 2026; Accepted 13 June 2026

Available online 23 June 2026

1. Introduction

The human brain is increasingly understood as a complex system whose remarkable computational capabilities arise not from the activity of isolated regions but from the coordinated interplay of distributed neural ensembles [1,2]. Functional magnetic resonance imaging (fMRI) has become an indispensable tool for probing this organization, offering a non-invasive window into the brain's functional architecture through the blood oxygenation level-dependent (BOLD) signal [3,4]. Over the past two decades, network neuroscience has provided a powerful framework for analyzing fMRI data, modeling the brain as a graph where nodes represent brain regions and edges capture pairwise functional connectivity—typically quantified by measures such as Pearson correlation or coherence [5,6]. This perspective has yielded fundamental insights into principles of brain organization, including small-world topology, modular structure, and the existence of highly connected hubs, while also revealing alterations associated with neurological and psychiatric disorders [7–11].

Despite its transformative impact, the conventional graph-based paradigm rests on a fundamental simplifying assumption: that all functional interactions can be adequately captured by pairwise dependencies. This reductionist premise inherently excludes the possibility of polyadic interactions—emergent phenomena where the joint activity of three or more regions gives rise to information that cannot be decomposed into a sum of dyadic relationships [12,13]. A growing body of evidence, however, suggests that such higher-order interactions (HOIs) are not merely a theoretical curiosity but constitute a core computational primitive underlying complex cognitive functions, including multi-sensory integration, decision-making, and executive control [14–16]. The recognition that brain function may be fundamentally shaped by these multi-body interactions has catalyzed a paradigm shift, motivating the development of analytical frameworks capable of moving beyond pairwise connectivity [17].

Recent methodological advances have begun to address this challenge, drawing on tools from algebraic topology, information theory, and multivariate statistics [18–21]. As comprehensively reviewed in Ref. [22], approaches based on hypergraphs and simplicial complexes have proven particularly promising for capturing the rich landscape of HOIs in fMRI data, revealing synergistic interactions invisible to standard functional connectivity analyses and offering superior sensitivity in distinguishing clinical populations. This evolution in analytical methodology aligns with a broader trend in complex network science, where the study of HOIs has emerged as a frontier for understanding emergent collective phenomena across diverse domains, from social networks to biological systems [23–25].

While these developments have established the conceptual and mathematical foundations for HOI analysis, a critical methodological gap remains: the effective integration of such representations with powerful learning frameworks. Classical approaches to HOI detection, while valuable for hypothesis testing, often rely on predefined rules for hyperedge construction and do not directly leverage the predictive power of modern machine learning. In parallel, the field of graph representation learning has witnessed remarkable progress with the advent of Graph Neural Networks (GNNs), which learn expressive node embeddings through message passing and have achieved state-of-the-art performance in node classification, link prediction, and graph classification tasks [26,27]. GNNs have shown high efficiency for solving engineering tasks [28] and processing experimental data [29], including functional brain networks [30,31]. However, GNNs are inherently limited to pairwise graph structures and cannot directly operate on hypergraphs without substantial adaptation.

A pivotal development in bridging this gap came with the introduction of UniGNN — a unified framework that generalizes classical GNN architectures to hypergraphs by reinterpreting message passing as a two-stage aggregation process [32]. Within this framework, information is first aggregated within hyperedges and then across incident hyperedges, enabling the direct application of well-established GNN designs such as GCN, GAT, GIN, and GraphSAGE to hypergraph-structured data. This conceptual unification not only extends the expressive power of GNNs to higher-order representations but also facilitates the incorporation of sophisticated architectural innovations — including mechanisms to mitigate over-smoothing in deep networks — into hypergraph learning. UniGNN has demonstrated substantial performance gains over existing hypergraph neural networks (HGNNs) across multiple benchmark datasets, establishing its potential as a foundational tool for hypergraph representation learning.

The convergence of these developments — the neuroscientific imperative to characterize HOIs, the mathematical framework of hypergraphs for representing them, and the computational power of HGNNs for learning from them — creates an opportunity for advancing our understanding of brain function and dysfunction. However, to date, the application of UniGNN-like architectures to fMRI-based functional brain networks has remained largely unexplored. Key questions remain unanswered: How effectively can HGNNs capture clinically relevant HOI patterns from fMRI data? How do their classification performance and the interpretability of their learned representations compare with traditional pairwise approaches? What insights into network organization can be gleaned from the hypergraph structures identified by these models?

This study aims to address these issues by systematically evaluating the application of HGNNs for classifying functional brain networks derived from resting-state fMRI data for individuals with autism spectrum disorders (ASD) using an open-source dataset ABIDE [33]. We construct hypergraph representations of brain functional connectivity using Lasso-based hyperconnectivity extraction technique [34,35] and implement two highly advanced and optimized variants of the UniGNN architecture (UniGCN and UniGIN) [32] to learn discriminative embeddings capable of capturing HOIs. We compare their performance with traditional machine learning methods and classical deep GNN applied to pairwise interactions. Furthermore, we analyze the learned hypergraph structures to identify brain regions and cross-region interaction patterns that contribute most to classification decisions and relate these results to established principles of brain network organization using a consensus network-based approach [36,37] adapted to hypergraphs.

This work is situated within a broader scientific context that has been profoundly shaped by the contributions of Professor Stefano Boccaletti. Over the past decades, Prof. Boccaletti has played a significant role in the development of complex systems

science, making seminal contributions to our understanding of synchronization, network dynamics, and, crucially, the physics of HOIs [24,38,39]. His pioneering work on the structure and dynamics of complex networks has inspired generations of researchers and laid much of the theoretical groundwork upon which the present study builds. Beyond his scientific contributions, his sustained support and encouragement for interdisciplinary research bridging physics, neuroscience, and complex network theory have been instrumental in nurturing the community that now explores these frontiers. It is therefore a particular honor to contribute to this special issue celebrating his 60th birthday, and we hope that this work reflects the spirit of innovation and intellectual generosity that he has so consistently embodied.

2. Methods

2.1. Dataset

The Autism Brain Imaging Data Exchange I (ABIDE I) is a large-scale, multi-site collection of resting-state functional magnetic resonance imaging (rs-fMRI) and structural MRI data, designed to facilitate the study of brain connectivity in autism spectrum disorder (ASD). The initial release (ABIDE I) involves 17 international sites, yielding over 1000 samples of rs-fMRI data, spanning a wide age range and varying acquisition protocols [33].

In this study, we used data from the ABIDE Preprocessed repository [40], which contains ABIDE data preprocessed using several pipelines. We selected the preprocessing strategy performed using the Data Processing Assistant for Resting-State fMRI (DPARSF) [41], with bandpass filtering and global signal regression applied. Finally, we used BOLD time series parcellated into $M = 116$ regions of interest (ROIs) using the AAL atlas [42]. A total of 884 samples were loaded from the repository, including 408 ASD and 476 typically developing (TD) subjects.

2.2. Pairwise functional connectivity assessment

For each subject, we estimated pairwise functional connectivity between all ROI pairs using the Pearson correlation coefficient, resulting in a symmetric connectivity matrix $A = M \times M$ per subject. Pearson correlation is a widely used measure of statistical dependence in rs-fMRI studies and reflects temporal synchrony between spatially distinct brain regions. To reduce noise-driven connections, the statistical significance of each correlation coefficient was assessed, and all connections not meeting the significance threshold of $p < 0.05$ were set to zero.

2.3. Hypergraphs assessment

Although the graph-based models have revealed many fundamental principles of cortical organization, they inherently assume that all functional interactions in the brain network are pairwise. However, brain functional connectivity exhibits behavior that goes beyond the scope of pairwise connections [12,43].

In the present study, each subject's data was transformed into a hypergraph representation using sparse group lasso (SGL) method [44].

In accordance with the methodology, we treat each BOLD time series y_m of ROI m as a sparse linear combination of all other ROIs: $y_m = X_m\beta_m + \tau_m$, where X_m is a predictor matrix containing all other ROIs except of mth and β_m is a coefficient vector determining the degree of influence of ROIs in X_m on the ROI m; τ_m is the noise term. The non-zero values of β_m indicate the members of hyperedge "centered" in the ROI m [45]. Then, we define the partitioning of the elements in X_m into G pre-determined anatomical groups derived from the AAL atlas anatomical labeling framework: central, parietal, frontal, temporal lobes, limbic node, cerebellum, vermis, insula and subcortical grei nuclei [46]. For each ROI m, SGL estimates the coefficient vector β_m:

$$\hat{\beta}^{(m)} = \arg\min_{\beta} \frac{1}{2n}\|y^{(m)} - X^{(m)}\beta\|_2^2 + (1-\alpha)\lambda \sum_{g=1}^{G} \sqrt{p_g}\|\beta_{G_g}\|_2 + \alpha\lambda\|e\|_1, \tag{1}$$

where n is the number of time points in the BOLD time series, $\lambda \geq 0$ is a regularization strength that controls the sparsity of the model. The second term of this equation represents the group $\frown_2$ penalty that introduces the group sparsity: here, β_{G_g} corresponds to the subvector of coefficients belonging to the group g, p_g is a size of the group g. The third term corresponds to the elementwise l_1 penalty, which is a standard lasso penalty that encourages the within-group sparsity. A measure $\alpha \in [0, 1]$ controls the balance between these two penalties: $\alpha = 0$ gives the group lasso, $\alpha = 1$ gives the lasso, and $0 < \alpha < 1$ combines both. In this research, both α and λ were set to 0.1.

Estimation of β_m, $m \in 1, \ldots, M$, was performed for each subject. The subsets of non-zero values of β_m were interpreted as a hyperedge $e \in E$ 'centered' at the node m. Then, we removed empty hyperedges, subedges and calculated the similarity of the remaining hyperedges to reduce structural duplication. Similarity was defined using the Jaccard coefficient

$$J(e_i, e_j) = \frac{|e_i \cap e_j|}{|e_i \cup e_j|}. \tag{2}$$

Hyperedges exceeding a predefined similarity threshold of 0.9 were merged.

Finally, each subject was represented by a hypergraph in the form of a single incidence matrix $H^s \in \{0, 1\}^{M \times N_s}$, where N_s denotes the number of retained hyperedges for subject s, which was comparable across subjects and groups.

2.4. Machine learning

To evaluate the discriminative power of the obtained representations, we employed multiple machine learning (ML) models spanning different methodological families. Each model was trained and evaluated using a stratified k-fold cross-validation scheme with $k = 5$ to ensure robustness. Model performance was assessed using the F1-score and the area under the ROC curve (AUC), computed on held-out data. Hyperparameters were optimized using nested cross-validation within the training folds.

2.4.1. Support vector machine (SVM)

As a baseline approach, we employed an SVM classifier. For each subject, we obtained the degrees of nodes of the corresponding hypergraph by calculating the number of hyperedges that each of M nodes belongs to and used these vectorized representations to train the model. The best performance was achieved using a model with a radial basis function (RBF) kernel, with $\gamma = 0.1$ and a regularization parameter of $C = 1$.

2.4.2. Graph convolutional network (GCN)

To explicitly model the network structure of brain functional relationships, we employed a graph convolutional network (GCN) with a single GCNConv layer [47] consisting of 64 hidden units, followed by batch normalization, a ReLU activation function, global max pooling, a multilayer perceptron (MLP) classifier, and dropout with a rate of 0.3. Each node i in each graph was represented by a feature vector constructed from summary connectivity measures $[s_i^+, s_i^-, s_i^{(abs)}, \mu_i^{(abs)}, \sigma_i, c_i]$, comprising:

1. s_i^+ – sum of strength of the positive connections of the node i,
2. s_i^- – sum of strength of the negative connections of the node i,
3. s_i^{abs} – sum of strength of all connections of the node i,
4. $\mu_i^{(abs)}$ – mean of absolute connections of the node i,
5. σ_i – standard deviation of connections of the node i,
6. c_i – correlation coefficient of the node i.

Additionally, we used the Adam optimizer with a learning rate of 1×10^{-4} and weight decay of 1×10^{-4}, along with a binary cross-entropy loss function and a sigmoid output layer.

2.4.3. Unified graph convolutional network (unignn)

To capture higher-order interactions beyond pairwise connections, we employed the UniGNN [32] message-passing framework, which generalizes graph neural networks to hypergraphs. In particular, we used the Unified Graph Convolutional Network (UniGCN) and the Unified Graph Isomorphism Network (UniGIN). Both models utilize a two-stage message aggregation process according to the following rule:

$$\begin{cases} h_e = \phi_1(\{x_j\}_{j \in e}), \\ \tilde{x}_i = \phi_2(x_i, \{h_e\}_{e \in E_i}) \end{cases} \tag{3}$$

where ϕ_1 and ϕ_2 are the aggregation functions for hyperedges and vertices, respectively. In the first stage, the messages are aggregated from all vertices belonging to a hyperedge e. In the second stage, each vertex is updated using the aggregated messages from its incident hyperedges.

UniGCN generalizes the message-passing process introduced for GCN [47] by incorporating normalization based on hyperedge degrees. UniGIN is a generalization of the Graph Isomorphism Network (GIN) that uses MLPs in its aggregation mechanisms, allowing it to capture higher-order structures.

For both models, we tested two node features parametrization strategies: (i) functional connectivity profiles and (ii) time series statistival descriptors, which capture, respectively, inter-ROI interaction patterns and intrinsic temporal characteristics of BOLD signals.

In the first approach, node features were determined directly from pairwise functional connectivity. Hence, for each subject, the ith ROI was represented by the ith row of the adjacency matrix A. In the second approach, the node features were derived from statistical properties of the corresponding BOLD signals. For each node i, four descriptive statistics were computed: $[\mu_i, \sigma_i, skew_i, kurt_i]$. The fist two correspond to the mean and the standard deviation of BOLD time series of ith node, the third corresponds to the skewness and the fourth — to the kurtosis.

2.5. Consensus network analysis

Group-level consensus networks were constructed for both pairwise and higher-order representations of brain functional networks.

For the pairvase graphs, the first step was to average the binarized connectivity matrices A across subjects:

$$\bar{A}^s = \frac{1}{S} \sum_{s=1}^{S} A^s, \tag{4}$$

where S is a number of subjects in the corresponding group (ASD or TD). Then, the consensus graph cG^s for the subject s with node set $V = v_1, \ldots, v_M$, $M = 116$ can be defined by an adjacency matrix cA^s:

$$cA^s_{i,j} = \begin{cases} 0, \text{if } \bar{A}^s_{i,j} < \gamma \\ 1, \text{otherwise} \end{cases} \tag{5}$$

where $\gamma = 0.8$ is the threshold, which means that the pairwise consensus network included edges present in at least 80% of subjects within each group. These steps allow the identification of functional connections that are consistently present across subjects in the considered groups.

For HOIs, we generalize this approach as follows. For each subject s, the hypergraph can be represented as an incidence matrix $H^s \in 0, 1M \times N^s$, where $M = 116$ is a number of ROIs and N^s is a number of hyperedges in the hypergraph H^s. At the first step, for all subjects, the hyperedges were pulled into a common set:

$$\varepsilon_G = \bigcup_{s \in G} \{e^s_1, \ldots, e^s_{N_s}\}, \tag{6}$$

where G is the subset of subjects corresponding to the considered group (ASD or TD). Since the hyperedges do not match exactly between subjects, we employed the similarity quantified by the Jaccard coefficient (2). The hyperedges e_i and e_j were considered equivalent if the corresponding Jaccard coefficient exceeded the pre-defined similarity threshold, which we chose to be 0.7.

The defined similarity allowed us to pool similar hyperedges observed across subjects into groups C_k, $k = 1, \ldots, N_g$, where N_g is a number of observed groups. For each node v, we calculated the frequency of its membership within the group C_k as:

$$f_{vk} = \frac{1}{|C_k|} \sum_{e \in C_k} 1_e(v), \tag{7}$$

where $1_e(v)$ is 1 if $v \in e$ and 0 otherwise — indicator function. We included the node into the consensus hyperedge if its f exceeded the pre-defined frequency threshold, which we set to be 0.6.

The final consensus hypergraph for the group G was represented by the incidence matrix $cH \in 0, 1^{m \times N_G *}$, where $N_G *$ is a number of obtained consensus hyperedges.

The resulting pairwise consensus networks included 143 edges for the ASD group and 164 edges for the TD group. The consensus hypergraphs included 11 hyperedges for the ASD group and 10 hyperedges for the TD group. Consensus hypergraphs for both groups are illustrated in Fig. 1.

2.6. Contrastive hypergraph analysis and mapping to large-scale networks

To systematically characterize the structural differences between group-level consensus hypergraphs and to relate the obtained hyperedges to known principles of brain organization, we performed a contrastive analysis and mapped each hyperedge to established large-scale brain networks (LSNs).

2.6.1. Contrastive analysis

Consensus hyperedges from the ASD and TD groups were compared using the Jaccard similarity coefficient (2). For each TD hyperedge, the best-matching ASD hyperedge was identified as the one maximizing Jaccard similarity. Hyperedge pairs with $J = 1.0$ were classified as *identical* (fully conserved across groups); pairs with $0.5 \leq J < 1.0$ as *partially overlapping*; and pairs with $J < 0.5$ as *divergent*. Hyperedges present in one group but lacking any close match ($J < 0.5$) in the other group were classified as group-specific.

2.6.2. Mapping to large-scale networks

Each AAL ROI was assigned to one of eight canonical LSNs based on established functional neuroanatomy [48–50]: the default mode network (DMN), central executive network (CEN), salience network (SN), sensorimotor network (SMN), visual network (VN), temporal/auditory network (TN), subcortical network (SC), and cerebellar network (CB). The complete mapping is provided in Table A.4 in the Appendix. For each consensus hyperedge, the LSN composition was computed as the number of constituent ROIs belonging to each LSN, yielding an LSN profile vector that characterizes the functional network content of the hyperedge.

All calculations were performed using the Python programming language. Pearson correlation was computed using the SciPy library [51]. Higher-order functional connectivity networks, SVM model, and consensus network algorithms were implemented using tools from the scikit-learn library [52]. UniGNN models were developed using the TopoModelX package [53].

3. Results

3.1. Machine learning classification

The performance of developed ML models is presented in Table 1.

Overall, the evaluated models demonstrated a pronounced hierarchy in discriminative performance, highlighting the critical role of both network representation and node feature parametrization.

The SVM baseline, which operated on vectorized hypergraph node degrees without leveraging the full network topology, achieved the lowest performance across all metrics (F1-score = 0.44, AUC = 0.54, balanced accuracy = 0.55). This result indicates that simple

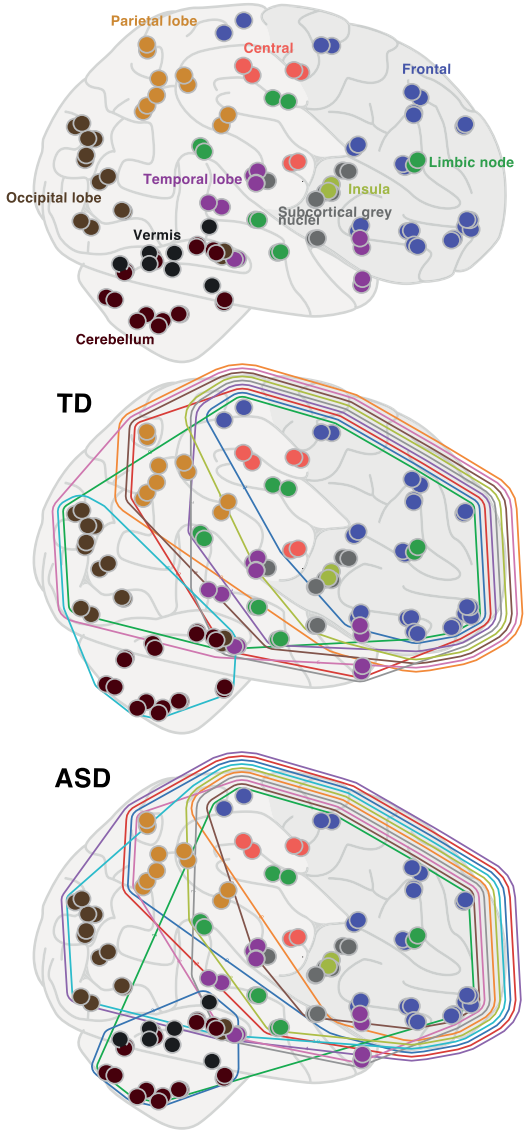

Fig. 1. Consensus hypergraph views for TD and ASD groups. The top panel depicts the ROIs location on the brain saggital view with labels corresponding to anatomical groups used to restore HOI; the color of the label corresponds to the color of nodes included in the corresponding group. The middle and lower panel shows consensus hypergraph structure obtained for TD and ASD group, respectively.

Table 1
Summary table of ML model performance.

Model	Node features	F1-score	AUC score	Balanced acc
SVM	–	0.44 ± 0.059	0.54 ± 0.047	0.55 ± 0.029
GCN	summary feats	0.59 ± 0.044	0.55 ± 0.043	0.54 ± 0.035
UniGCN	ts feats	0.62 ± 0.031	0.58 ± 0.072	0.59 ± 0.038
	pairwise feats	0.61 ± 0.041	0.59 ± 0.032	0.59 ± 0.033
UniGIN	ts feats	0.64 ± 0.026	0.74 ± 0.042	0.70 ± 0.039
	pairwise feats	0.77 ± 0.042	0.80 ± 0.048	0.76 ± 0.037

topological summaries of hypergraph structure, while informative for consensus-level group comparisons (see Section 3.2), carry insufficient discriminative power for individual-level classification. The GCN model, which explicitly incorporated pairwise graph structure via spectral convolutions and used summary connectivity features, yielded a moderate F1-score of 0.59 but exhibited a low AUC of 0.55 and balanced accuracy of 0.54, suggesting limited generalization and poor calibration despite the richer input representation.

Table 2
Comparison of the obtained results with state-of-the-art classification frameworks on ABIDE.

Study	Method	Score
Han and Li [54]	Unified Multi-View Hypergraph Learning (UMHL)	AUC = 0.75 ± 0.015
Mehul et al. [55]	Hypergraph neural model with learned hyperedges + gated attention	AUC = 0.7703 ± 0.0185
Han et al. [56]	Inter-Intra High-order Brain Network (I^2HBN)	AUC = 0.8378 ± 0.0111 (NYU); AUC = 0.8237 ± 0.0170 (UCLA)
Hao et al. [57]	Autoencoder + Broad Learning System	ACC = 0.718
Ours	**UniGIN**	**AUC = 0.80 ± 0.048**

The transition to hypergraph-based architectures produced consistent improvements. UniGCN achieved comparable F1-scores for both time series and pairwise connectivity features (0.62 and 0.61, respectively), with AUC values of 0.58 and 0.59. However, the most substantial performance gain was observed with UniGIN, which demonstrated a clear advantage attributable to the choice of node feature parametrization. When using time series statistical descriptors (mean, standard deviation, skewness, and kurtosis of BOLD signals, "ts feats" in Table 1), UniGIN achieved an F1-score of 0.64, AUC of 0.74, and balanced accuracy of 0.70. In contrast, when pairwise Pearson correlation profiles were used as node features ("pairwise feats" in Table 1), thereby encoding the full vector of each region's functional connectivity with all other regions, performance increased substantially, reaching an F1-score of 0.77, AUC of 0.80, and balanced accuracy of 0.76.

This pattern reveals two complementary insights. First, the superiority of UniGIN over UniGCN suggests that the more expressive aggregation mechanism of GIN, which employs MLPs and has been shown to be maximally powerful among message-passing neural networks [27], is better suited to exploiting the structural information encoded in hypergraphs.

Second, and more critically, the dramatic performance gap between the two node feature strategies within UniGIN (a 13-point improvement in F1-score and a 6-point gain in AUC when switching from time series features to pairwise connectivity features) demonstrates that the hypergraph structure alone is insufficient for optimal classification. Rather, the integration of pairwise functional connectivity profiles into the node feature space — effectively embedding the topology of dyadic interactions within the framework of higher-order structure — is essential for maximizing classification accuracy.

3.1.1. Comparison with the state-of-the-art on ABIDE

Table 2 reflects the current state-of-the-art results on ABIDE dataset classification with ML models specifically designed to perform on HOIs, including the results obtained in the current research. Although all papers report the accuracy/AUC metrics, the direct comparison of the results is limited due to the difference in ABIDE versions, subsets and parcellations under use. However, the large-scale review allows to determine that the reported AUC = 0.80 makes our results competitive with the current state-of-the-art on ABIDE.

3.2. Consensus network

The results in Table 1 indicate that node features derived from pairwise functional connectivity profiles consistently yielded better performance compared to the features based on BOLD time series. To study whether the reasons behind such behavior of HOI-based ML models may be reflected in a topological organization of functional connectivity networks, both pairwise and higher-order, we employed the consensus network approach, which has proved itself as a powerful tool that provides useful insights into group-level functional connectivity network structure [36,37].

We constructed consensus networks for both pairwise connectivity and higher-order (hypergraph) representations separately for ASD and TD groups. Fig. 2 shows the degree vectors for obtained topological structures.

The pairwise consensus network exhibits a considerable variability across ROIs and shows multiple localized peaks and fluctuations. The curves for ASD and TD groups have similar overall shape, with the differences observed at specific regions. Notably, several prominent peaks in the pairwise degree profile correspond to individual brain regions exhibiting strong local connectivity differences between groups, suggesting that ASD-related alterations at the pairwise level are regionally specific and distributed across multiple functional systems. Such localized differences in pairwise connectivity are consistent with established findings of region-specific dysconnectivity in ASD, including altered connectivity patterns involving the default mode, salience, and sensorimotor networks [58,59].

In contrast, the consensus hypergraph degree profile exhibits a qualitatively different organizational pattern. The degree curves show extended plateaus where the node degree of the ASD group is consistently higher than that of the TD group, reflecting the aggregation of nodes into shared hyperedges in accordance with the anatomical grouping of ROIs. This plateau structure indicates that HOIs in the ASD group involve broader recruitment of brain regions into group-level hyperedges, which may be interpreted as an expansion or over-engagement of large-scale functional modules. The more regularized, block-wise organization of node degrees in the hypergraph consensus, compared to the noisy, region-specific profile of pairwise consensus, suggests that hypergraph-level representations capture meso-scale organizational principles [11], corresponding to the coordinated activity of anatomically coherent brain subsystems, that are smoothed out or obscured at the level of individual pairwise connections.

Taken together, these results reveal a complementary structure: the pairwise consensus network highlights localized, region-specific connectivity differences between ASD and TD groups, while the consensus hypergraph captures broader, more systematic

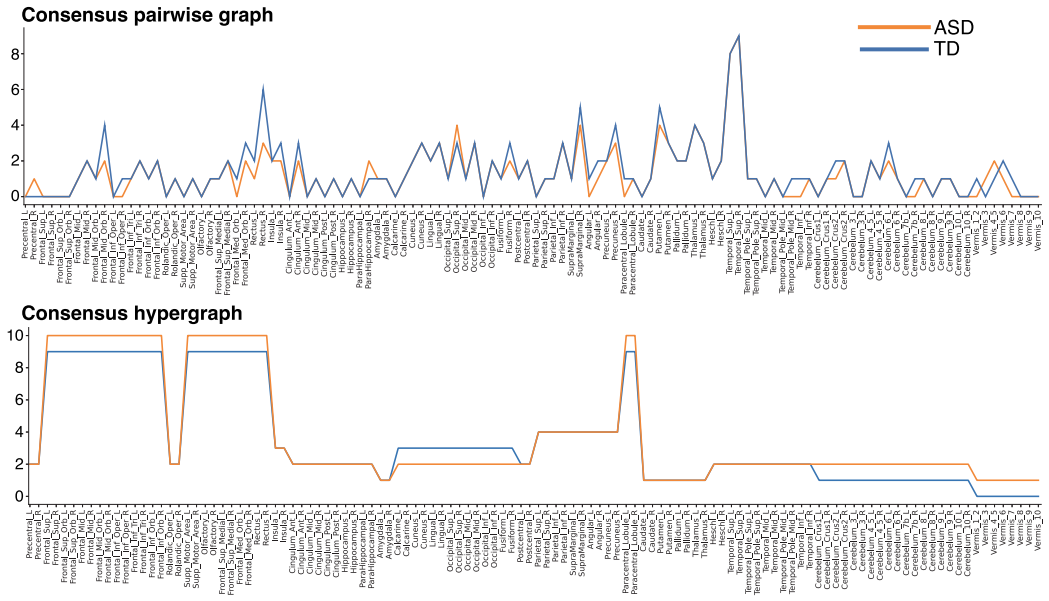

Fig. 2. Node degrees of consensus graph (upper panel) and consensus hypergraph (lower panel). The order of the brain regions corresponding to the areas of the anatomical atlas used is the same for both panels.

Table 3
Contrastive matching of consensus hyperedges (HEs) between TD and ASD groups. J denotes Jaccard similarity. Nine out of ten TD hyperedges have identical matches in ASD. The two bottom rows indicate the divergent pair and the ASD-specific hyperedge.

TD	ASD	J	LSN composition (dominant networks)
HE0	HE10	1.00	DMN + CEN + SN + VN + SMN
HE1	HE8	1.00	DMN + SN + SMN + CEN (sensorimotor–salience)
HE2	HE6	1.00	DMN + CEN + TN + SN (fronto-temporo-parietal)
HE3	HE9	1.00	DMN + CEN + SN (DMN-dominant, cingulo-hippocampal)
HE4	HE2	1.00	DMN + CEN + SN (DMN-dominant, extended: cingulate + parietal)
HE6	HE4	1.00	DMN + CEN + VN + SN (fronto-parieto-occipital)
HE7	HE7	1.00	DMN + SN + TN + CEN (fronto-insulo-temporal)
HE8	HE5	1.00	DMN + SN + SC + CEN (fronto-subcortical)
HE9	HE0	1.00	DMN + CEN + SN + SMN (fronto-parieto-motor)
HE5	HE3	0.45	*Divergent*: TD = VN + CB; ASD = CB only (+Vermis)
–	HE1	–	*ASD-specific*: Frontal core + CB (fronto-cerebellar)

divergences reflecting group-level modular organization of higher-order interactions. This dual characterization provides a multi-scale view of functional brain network alterations in ASD and offers a neurobiological basis for interpreting the superior classification performance of the UniGIN model when pairwise connectivity features are embedded within a hypergraph learning framework.

3.3. Contrastive hypergraph analysis and LSN mapping

To further characterize the structural correspondence and divergence between consensus hypergraphs, we performed a pairwise Jaccard matching and mapped each hyperedge to canonical LSNs. The results are summarized in Table 3.

The contrastive analysis revealed a striking degree of structural conservation: 9 out of 10 TD consensus hyperedges had a topologically identical match ($J = 1.0$) in the ASD consensus hypergraph, meaning that the constituent ROI sets were completely identical between groups. The LSN composition of all consensus hyperedges is visualized in Fig. 3.

All shared hyperedges contained a common frontal "core" comprising 24 frontal ROIs spanning the DMN (medial prefrontal cortex, orbitofrontal cortex, rectus), CEN (dorsolateral prefrontal cortex), and SN (inferior frontal gyrus, supplementary motor area) components, augmented by varying combinations of parietal, temporal, occipital, limbic, or subcortical regions that define the functional specificity of each hyperedge.

Despite this conserved backbone, two key structural differences emerged. First, the only non-matching pair (TD HE5 ↔ ASD HE3, $J = 0.45$) revealed a qualitative reorganization of the visual-cerebellar module. In TD, this hyperedge comprised 14 visual network

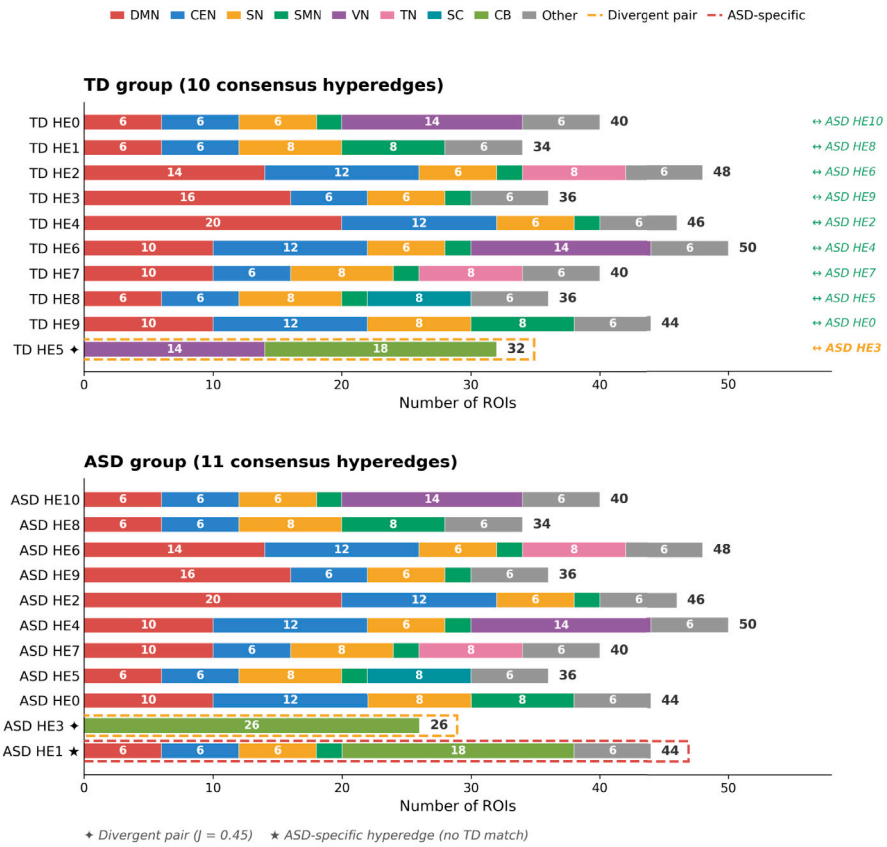

Fig. 3. Large-scale network (LSN) composition of consensus hyperedges for TD (top) and ASD (bottom) groups. Each horizontal bar represents one consensus hyperedge; colored segments indicate the number of ROIs belonging to each LSN. Arrows on the right of the TD panel indicate the matched ASD hyperedge ($J = 1.0$). Dashed orange border marks the divergent pair ($J = 0.45$); dashed red border marks the ASD-specific hyperedge with no TD counterpart. (For interpretation of the references to color in this figure legend, the reader is referred to the web version of this article.)

ROIs (calcarine, cuneus, lingual, occipital, fusiform) jointly with 18 cerebellar ROIs, reflecting a coordinated visuo-cerebellar higher-order interaction. In ASD, the visual component was entirely absent, and the hyperedge consisted exclusively of cerebellar regions, supplemented by all 8 Vermis subdivisions, yielding an isolated, purely cerebellar module of 26 ROIs.

Second, the ASD consensus hypergraph contained one additional hyperedge (ASD HE1) with no counterpart in TD. This ASD-specific hyperedge bridged the frontal core (24 ROIs: DMN, CEN, SN components) with the entire cerebellar network (18 ROIs), establishing a fronto-cerebellar higher-order coupling that was absent from the TD group.

Taken together, these findings indicate that while the overall higher-order modular architecture is largely conserved between ASD and TD, the ASD group exhibits (i) a decoupling of visual and cerebellar systems at the hypergraph level, (ii) the emergence of an isolated cerebellar module with expanded Vermis recruitment, and (iii) the formation of an aberrant fronto-cerebellar hyperedge. The Vermis ROIs (8 subdivisions) were exclusively present in the ASD consensus and entirely absent from the TD consensus, and the ASD consensus covered all 116 AAL ROIs compared to 108 in TD.

4. Discussion

This study presents a systematic evaluation of hypergraph neural networks for classifying functional brain networks in ASD, demonstrating that the joint modeling of higher-order hypergraph structure and pairwise connectivity features yields classification performance that substantially surpasses conventional graph-based and classical machine learning approaches. In this section, we discuss the key findings in the context of existing literature, consider their neuroscientific implications, and address the limitations and future directions of this work.

4.1. Multiscale integration drives classification performance

The central finding of this study is that neither higher-order structure alone nor pairwise connectivity alone suffices for optimal ASD classification. Rather, it is the synergistic combination of both scales of functional interaction — encoded through hypergraph

topology (capturing group-level, polyadic relationships) and pairwise connectivity profiles (capturing local, dyadic dependencies) — that produces the most discriminative representation. This conclusion is supported by the systematic ablation across model architectures and feature strategies summarized in Table 1.

The SVM baseline, which relied solely on hypergraph node degrees without modeling network topology, demonstrated near-chance performance (AUC = 0.54), confirming that scalar summaries of hypergraph structure are insufficient for individual-level discrimination. The GCN model, which operated exclusively on pairwise graphs with summary features, achieved moderate F1-scores (0.59) but similarly low AUC (0.55), illustrating the limitations of purely dyadic representations even when processed through learned graph convolutions. These results are consistent with the broader literature on ASD classification using the ABIDE dataset, where specially optimized GNN-based approaches applied to pairwise functional connectivity typically achieve accuracies in the range of 65–75% [60,61], with more recent methods reaching up to approximately 80% when incorporating additional strategies such as phenotypic feature fusion, domain adaptation, or multi-view learning [62,63].

The hypergraph-based UniGNN models demonstrated a clear advantage over their pairwise counterparts. However, a crucial observation is that the choice of node features had a dramatic impact on performance. UniGIN with time series statistical descriptors achieved an AUC of 0.74, whereas the same architecture with pairwise functional connectivity profiles as node features reached an AUC of 0.80 — a substantial improvement that highlights the importance of embedding dyadic interaction patterns within the hypergraph learning framework. This finding underscores a key methodological insight: the hypergraph structure defines the higher-order topological scaffold, essentially delineating which groups of brain regions interact jointly, while the pairwise connectivity profiles provide the fine-grained relational information that characterizes how individual regions within and across these groups are functionally coupled. Both levels of description are necessary for a complete and discriminative representation.

4.2. Neuroscientific interpretation: bridging scales of brain organization

The complementary roles of hypergraph structure and pairwise features in our framework resonate strongly with established principles of multiscale brain network organization. It is well recognized that the brain is organized hierarchically, with large-scale networks (LSNs), such as the default mode, salience, and central executive networks, serving as meso-scale modules that coordinate the activity of their constituent brain regions [1,49]. Within each LSN, pairwise functional connections define the internal wiring that supports specialized information processing, while interactions among LSNs reflect higher-order coordination that underpins complex cognitive functions [2,11]. The disruption of both intra-network and inter-network connectivity has been repeatedly implicated in ASD, with evidence for reduced functional segregation and integration [6,59,64].

In our framework, the sparse group lasso (SGL)-derived hyperedges can be interpreted as data-driven approximations of such meso-scale functional modules. The SGL method enforces both regional sparsity and anatomical group structure, producing hyperedges that reflect coordinated multi-region activity patterns aligned with the known parcellation of the brain into functional subsystems. By using these hyperedges as the structural backbone for UniGIN, the model captures group-level (polyadic) interactions that correspond to the coordinated engagement of distributed brain systems. Simultaneously, embedding pairwise Pearson correlation profiles as node features preserves the fine-grained topology of dyadic functional connections within and between these modules. This dual encoding thus provides the model with information at two complementary spatial scales: the broad, modular organization captured by hypergraph topology, and the detailed, region-specific connectivity captured by pairwise features.

This multi-scale perspective is further supported by the consensus network analysis (see Fig. 2). The pairwise consensus graph revealed numerous localized peaks in node degree, reflecting strong region-specific connectivity differences between ASD and TD groups distributed across multiple functional systems. In contrast, the consensus hypergraph exhibited extended plateau structures with consistently higher node degrees in the ASD group, corresponding to the broader engagement of anatomically coherent brain regions into shared hyperedges. These plateau patterns suggest an over-recruitment or expansion of large-scale functional modules in ASD at the meso-scale level, while the localized pairwise differences point to more specific intra-module and inter-region dysconnectivity. The coexistence of these two patterns — stable, structured group differences at the hypergraph level and variable, region-specific differences at the pairwise level — mirrors the known duality of ASD neuropathology, which involves both system-level organizational anomalies and focal connectivity alterations [59,64].

The synergy between these two scales of representation directly explains why UniGIN with pairwise features outperforms all other configurations. By constructing hypergraphs, we define the clusters and group-level interactions in the brain (hyperedges) and leverage them in UniGIN's message-passing mechanism. By embedding pairwise connectivity profiles as node features, we retain and propagate the underlying topology of dyadic interactions through these higher-order structures. This combined representation captures the maximum amount of information about brain function and dysfunction across multiple organizational scales, resulting in substantially improved classification accuracy.

This interpretation aligns with a growing body of evidence demonstrating that multi-scale approaches to brain network analysis provide superior sensitivity for detecting pathological alterations. Recent studies in the context of related neurodevelopmental and neuropsychiatric conditions have shown that the integration of pairwise and higher-order interaction descriptors yields more informative biomarkers than either representation alone [11,22]. Furthermore, emerging work on multi-view frameworks that combine pairwise functional connectivity with higher-order representations has demonstrated state-of-the-art classification performance across multiple brain disorder datasets [63,65], corroborating the principle that both scales of interaction carry complementary diagnostic information.

4.3. Cerebellar reorganization as an ASD-specific higher-order signature

The contrastive analysis of consensus hypergraphs (Section 3.3, Fig. 3) revealed that, despite a remarkably conserved higher-order backbone shared between ASD and TD groups, the primary structural divergence involves the cerebellum and its interactions with other brain systems. Three converging observations support this conclusion.

First, the only divergent hyperedge pair (TD HE5 vs. ASD HE3) showed a qualitative shift: in TD, visual and cerebellar regions formed a joint hyperedge, whereas in ASD the visual component was entirely absent, replaced by an expanded, purely cerebellar module incorporating all Vermis subdivisions. This visuo-cerebellar decoupling suggests a disruption in the higher-order coordination between posterior cortical processing (visual network) and cerebellar circuits in ASD. Such a pattern is consistent with reports of reduced cerebro-cerebellar functional connectivity in ASD [66] and may relate to the visuomotor processing atypicalities frequently observed in this population.

Second, the ASD-specific hyperedge (ASD HE1) that bridged frontal executive regions with the cerebellum represents an aberrant fronto-cerebellar higher-order coupling not observed in TD. This finding is particularly noteworthy given the growing recognition of cerebellar contributions to cognitive and social functions [50,67]. Disrupted cerebro-cerebellar connectivity has been identified as a hallmark of ASD across multiple studies [66,68], but these findings have been largely based on pairwise functional connectivity. Our results extend this body of evidence to the higher-order domain, demonstrating that cerebellar dysconnectivity in ASD manifests not only as altered pairwise links but also as a reorganization of the polyadic interaction structure.

Third, the exclusive presence of all 8 Vermis subdivisions in the ASD consensus (absent in TD) points to an expansion of the cerebellar module that recruits midline structures implicated in motor coordination, affective processing, and autonomic regulation. The Vermis has been specifically implicated in ASD pathophysiology, with structural and functional abnormalities reported in postmortem and neuroimaging studies.

Importantly, these cerebellar-specific differences coexist with a highly conserved "triple network" backbone. All shared hyperedges contain components of the DMN, CEN, and SN — the three networks forming the triple network model of psychopathology [49]. The preservation of this core structure suggests that higher-order organization among the principal cognitive networks remains largely intact in ASD at the group level, and that the primary disruption occurs at the interface between these networks and the cerebellum. This finding has implications for the interpretation of classification results: the discriminative information captured by UniGIN likely derives not from differences in the higher-order organization of canonical cognitive networks *per se*, but from the atypical cerebellar engagement and its altered coupling patterns with frontal and visual systems.

4.4. The role of model expressiveness

Beyond the feature engineering perspective, the architectural properties of UniGIN played a significant role in achieving the best performance. UniGIN builds upon the Graph Isomorphism Network (GIN) [27], which has been shown to be as powerful as the Weisfeiler–Lehman graph isomorphism test for distinguishing graph structures. In the hypergraph setting, UniGIN employs MLPs within its aggregation functions, enabling the model to learn non-linear transformations that capture complex patterns in both the within-hyperedge aggregation (messages from vertices to hyperedge) and the cross-hyperedge aggregation (messages from hyperedges to vertex). This is in contrast to UniGCN, which relies on normalization-based aggregation and achieved comparable but lower performance regardless of the node feature strategy used.

The higher expressiveness of UniGIN becomes particularly relevant when processing rich, high-dimensional node features (116-dimensional pairwise connectivity profiles). The MLP-based aggregation can effectively leverage subtle patterns in these feature vectors that linear normalization-based methods cannot exploit. This observation is consistent with the theoretical analysis in [27,32] and suggests that as the complexity and dimensionality of node representations increase, more expressive aggregation mechanisms are required to fully capitalize on the available information.

4.5. Comparison with the state-of-the-art

The best classification performance achieved by UniGIN (F1 = 0.77, AUC = 0.80, balanced accuracy = 0.76) is competitive with recent state-of-the-art results on the ABIDE dataset, as summarized in Table 2. Earlier deep learning studies on the full ABIDE I cohort reported accuracies around 70% [69], while more recent GNN- and hypergraph-based approaches have achieved AUC values of 0.75–0.84 depending on the atlas, sample selection, and whether additional information is incorporated [55,56]. The application of the UniGNN framework to the ABIDE dataset — and specifically the investigation of the interplay between hypergraph structure and node feature parametrization — has not been previously reported.

It is important to note that our results are obtained using a rigorously validated pipeline with nested cross-validation, without the use of phenotypic information, multi-modal data, or data augmentation strategies that have been employed in some studies reporting higher performance figures. The use of stratified 5-fold cross-validation with nested hyperparameter tuning ensures that our performance estimates are unbiased and generalizable, making direct comparison with studies using less stringent validation protocols difficult. Within this rigorous evaluation framework, the performance of UniGIN with pairwise features represents a substantial improvement over both classical baselines and standard graph-based approaches.

4.6. Limitations and future directions

Several limitations of the present study should be acknowledged. First, the ABIDE dataset, while providing a large and heterogeneous sample, is characterized by substantial inter-site variability in acquisition protocols, scanner hardware, and demographic composition. Although this heterogeneity increases the ecological validity of our results, it may also introduce confounding effects that could be mitigated through explicit site harmonization or domain adaptation techniques. Future work could explore the combination of UniGIN-based hypergraph learning with site-aware normalization or federated learning strategies to further improve generalizability across acquisition sites.

Second, the current study employs a static functional connectivity framework, computing pairwise correlations and hypergraph structures from the full time series of each subject. Dynamic approaches that capture temporal fluctuations in both pairwise and higher-order connectivity could reveal additional clinically relevant information and further improve classification performance [70].

Third, while the consensus network analysis provides valuable group-level insights into topological differences, a more detailed region-level and hyperedge-level analysis of the learned UniGIN representations, e.g. through attention-based interpretability or gradient-based feature attribution methods, could identify specific brain circuits and higher-order motifs most relevant for ASD classification.

Finally, although our framework demonstrates the benefits of integrating pairwise and higher-order representations, the current approach encodes these two scales sequentially (pairwise features as node attributes within a separately constructed hypergraph). Future architectures that jointly learn both the hypergraph structure and the pairwise feature transformation in an end-to-end manner could further optimize the balance between these complementary sources of information [65].

5. Conclusion

This study demonstrates that hypergraph neural networks, specifically UniGIN, provide a powerful framework for classifying functional brain networks in autism spectrum disorder when the complementary information from both higher-order and pairwise interaction scales is effectively integrated. The key finding is that optimal classification performance (F1 = 0.77, AUC = 0.80) is achieved only when pairwise functional connectivity profiles are embedded as node features within a hypergraph representation. Neither the hypergraph structure alone nor pairwise graph analysis alone yields comparable results.

This observation has a clear neuroscientific interpretation: the hypergraph captures meso-scale modular organization of the brain, delineating groups of regions that interact collectively, while pairwise connectivity features encode the fine-grained topology of dyadic functional relationships within and between these modules. Together, they provide a multi-scale representation that preserves the maximum amount of information about brain function and its disruption in ASD.

Consensus network analysis further supports this interpretation, revealing that group-level differences between ASD and typically developing subjects are structured and systematic at the hypergraph level but region-specific and localized at the pairwise level. The contrastive analysis of consensus hypergraphs identified the cerebellum as the primary locus of higher-order reorganization in ASD: visual-cerebellar decoupling, emergence of an isolated cerebellar module with expanded Vermis recruitment, and formation of an aberrant fronto-cerebellar hyperedge — all against a background of a highly conserved triple-network (DMN–CEN–SN) backbone.

These results establish a methodological principle for the application of higher-order network models in computational neuroscience and clinical neuroimaging: advancing beyond pairwise interactions requires not the replacement of dyadic analysis but its integration within richer, multi-scale topological frameworks. Future work extending this approach to dynamic connectivity, multimodal imaging, and other neurological and psychiatric conditions holds significant promise for the development of interpretable and clinically actionable biomarkers of brain network dysfunction.

CRediT authorship contribution statement

Elena N. Pitsik: Writing – original draft, Visualization, Validation, Software, Methodology, Investigation, Data curation. **Semen A. Kurkin:** Writing – original draft, Visualization, Validation, Software, Methodology, Investigation, Formal analysis, Conceptualization. **Alexander E. Hramov:** Writing – review & editing, Validation, Supervision, Project administration, Methodology, Investigation, Formal analysis, Conceptualization.

Declaration of competing interest

The authors declare that they have no known competing financial interests or personal relationships that could have appeared to influence the work reported in this paper.

The author is an Editorial Board Member/Editor-in-Chief/Associate Editor/Guest Editor for this journal and was not involved in the editorial review or the decision to publish this article.

Appendix. AAL ROI to large-scale network mapping

See Table A.4.

Table A.4
Assignment of AAL atlas ROIs to canonical large-scale brain networks (LSNs) used for consensus hyperedge characterization. Bilateral ROIs (_L, _R) are listed once. Mapping is based on established functional neuroanatomy [48–50].

LSN	AAL ROIs
DMN	Frontal_Sup_Medial, Frontal_Med_Orb, Cingulum_Ant, Cingulum_Mid, Cingulum_Post, Precuneus, Angular, Hippocampus, ParaHippocampal, Temporal_Pole_Sup, Temporal_Pole_Mid, Rectus
CEN	Frontal_Mid, Frontal_Mid_Orb, Frontal_Inf_Tri, Parietal_Sup, Parietal_Inf, SupraMarginal
SN	Insula, Frontal_Inf_Oper, Frontal_Inf_Orb, Supp_Motor_Area, Amygdala
SMN	Precentral, Postcentral, Rolandic_Oper, Paracentral_Lobule
VN	Calcarine, Cuneus, Lingual, Occipital_Sup, Occipital_Mid, Occipital_Inf, Fusiform
TN	Heschl, Temporal_Sup, Temporal_Mid, Temporal_Inf
SC	Caudate, Putamen, Pallidum, Thalamus
CB	Cerebelum_Crus1, Cerebelum_Crus2, Cerebelum_3, Cerebelum_4_5, Cerebelum_6, Cerebelum_7b, Cerebelum_8, Cerebelum_9, Cerebelum_10, Vermis_1_2, Vermis_3, Vermis_4_5, Vermis_6, Vermis_7, Vermis_8, Vermis_9, Vermis_10
Other	Frontal_Sup, Frontal_Sup_Orb, Olfactory

Data availability

Data will be made available on request.

References

[1] Bassett DS, Sporns O. Network neuroscience. Nature Neurosci 2017;20:353–64.
[2] Park H-J, Friston K. Structural and functional brain networks: from connections to cognition. Science 2013;342:1238411.
[3] Biswal BB, Uddin LQ. The history and future of resting-state functional magnetic resonance imaging. Nature 2025;641:1121–31.
[4] Logothetis NK. The underpinnings of the bold functional magnetic resonance imaging signal. J Neurosci 2003;23:3963–71.
[5] Bullmore E, Sporns O. Complex brain networks: graph theoretical analysis of structural and functional systems. Nature Rev Neurosci 2009;10:186–98.
[6] Hramov AE, Frolov NS, Maksimenko VA, Kurkin SA, Kazantsev VB, Pisarchik AN. Functional networks of the brain: from connectivity restoration to dynamic integration. Physics–Uspekhi 2021;64:584–616.
[7] Wang J, Zuo X, He Y. Graph-based network analysis of resting-state functional mri. Front Syst Neurosci 2010;4:16.
[8] Hallquist MN, Hillary FG. Graph theory approaches to functional network organization in brain disorders: A critique for a brave new small-world. Netw Neurosci 2018;3:1–26.
[9] Xia M, Womer FY, Chang M, Zhu Y, Zhou Q, Edmiston EK, Jiang X, Wei S, Duan J, Xu K, et al. Shared and distinct functional architectures of brain networks across psychiatric disorders. Schizophr Bull 2019;45:450–63.
[10] Khorev VS, Kurkin SA, Zlateva G, Paunova R, Kandilarova S, Maes M, Stoyanov D, Hramov AE. Disruptions in segregation mechanisms in fMRI-based brain functional network predict the major depressive disorder condition. Chaos Solitons Fractals 2024;188:115566.
[11] Kurkin S, Mayorova L, Khorev V, Pitsik E, Radutnaya M, Bondar E, Hramov A. Multiscale fmri analysis reveals hierarchical network disruptions underlying disorders of consciousness. Chaos Solitons Fractals 2025;200:117008.
[12] Battiston F, Cencetti G, Iacopini I, Latora V, Lucas M, Patania A, Young J-G, Petri G. Networks beyond pairwise interactions: Structure and dynamics. Phys Rep 2020;874:1–92.
[13] Giusti C, Ghrist R, Bassett DS. Two's company, three (or more) is a simplex: Algebraic-topological tools for understanding higher-order structure in neural data. J Comput Neurosci 2016;41:1–14.
[14] Luppi AI, Mediano PA, Rosas FE, Holland N, Fryer TD, O'Brien JT, Rowe JB, Menon DK, Bor D, Stamatakis EA. A synergistic core for human brain evolution and cognition. Nature Neurosci 2022;25:771–82.
[15] Varley TF, Pope M, Grazia J, Sporns O. Partial entropy decomposition reveals higher-order information structures in human brain activity. Proc Natl Acad Sci 2023;120:e2300888120.
[16] Santoro A, Battiston F, Lucas M, Petri G, Amico E. Higher-order connectomics of human brain function reveals local topological signatures of task decoding, individual identification, and behavior. Nat Commun 2024;15:10244.
[17] Battiston F, Amico E, Barrat A, Bianconi G, de Arruda G Ferraz, Franceschiello B, Iacopini I, Kéfi S, Latora V, Moreno Y, et al. The physics of higher-order interactions in complex systems. Nat Phys 2021;17:1093–8.
[18] Millán AP, Sun H, Giambagli L, Muolo R, Carletti T, Torres JJ, Radicchi F, Kurths J, Bianconi G. Topology shapes dynamics of higher-order networks. Nat Phys 2025;21:353–61.
[19] Smirnov N, Kurkin S, Hramov AE. A q-analysis package for higher-order interactions analysis in python and its application in network physiology. Front Netw Physiol 2025;5:1691159.
[20] Hindriks R, Broeders TA, Schoonheim MM, Douw L, Santos F, van Wieringen W, Tewarie PK. Higher-order functional connectivity analysis of resting-state functional magnetic resonance imaging data using multivariate cumulants. Hum Brain Mapp 2024;45:e26663.
[21] Rosas FE, Mediano PA, Gastpar M, Jensen HJ. Quantifying high-order interdependencies via multivariate extensions of the mutual information. Phys Rev E 2019;100:032305.
[22] Kurkin SA, Pisarchik AN, Mayorova LA, Hramov AE. Evolution of methods for assessing fmri-based functional networks: from classical pairwise connectivity to higher-order interactions. Phys Rep 2026;1174:1–66.

[23] Battiston F, Capraro V, Karimi F, Lehmann S, Migliano AB, Sadekar O, Sánchez A, Perc M. Higher-order interactions shape collective human behaviour. Nat Hum Behav 2025;1–17.
[24] Boccaletti S, Lellis P De, del Genio CI, Alfaro-Bittner K, Criado R, Jalan S, Romance M. The structure and dynamics of networks with higher order interactions. Phys Rep 2023;1018:1–64.
[25] Benson AR, Gleich DF, Leskovec J. Higher-order organization of complex networks. Science 2016;353:163–6.
[26] Kipf TN, Welling M. Semi-supervised classification with graph convolutional networks. In: International conference on learning representations. 2017, URL https://openreview.net/forum?id=SJU4ayYgl.
[27] Xu K, Hu W, Leskovec J, Jegelka S. How powerful are graph neural networks?. 2018, arXiv preprint arXiv:1810.00826.
[28] Jiang C, Chen N-Z. Graph neural networks (gnns) based accelerated numerical simulation. Eng Appl Artif Intell 2023;123:106370.
[29] Liang F, Qian C, Yu W, Griffith D, Golmie N. Survey of graph neural networks and applications. Wirel Commun Mob Comput 2022;2022:9261537.
[30] Bessadok A, Mahjoub MA, Rekik I. Graph neural networks in network neuroscience. IEEE Trans Pattern Anal Mach Intell 2022;45:5833–48.
[31] Pitsik EN, Maximenko VA, Kurkin SA, Sergeev AP, Stoyanov D, Paunova R, Kandilarova S, Simeonova D, Hramov AE. The topology of fmri-based networks defines the performance of a graph neural network for the classification of patients with major depressive disorder. Chaos Solitons Fractals 2023;167:113041.
[32] Huang J, Yang J. Unignn: a unified framework for graph and hypergraph neural networks. 2021, arXiv preprint arXiv:2105.00956.
[33] Martino A Di, Yan C-G, Li Q, Denio E, Castellanos FX, Alaerts K, Anderson JS, Assaf M, Bookheimer SY, Dapretto M, et al. The autism brain imaging data exchange: towards a large-scale evaluation of the intrinsic brain architecture in autism. Mol Psychiatry 2014;19:659–67.
[34] Jie B, Wee C-Y, Shen D, Zhang D. Hyper-connectivity of functional networks for brain disease diagnosis. Med Image Anal 2016;32:84–100.
[35] Li Y, Liu J, Gao X, Jie B, Kim M, Yap P-T, Wee C-Y, Shen D. Multimodal hyper-connectivity of functional networks using functionally-weighted LASSO for MCI classification. Med Image Anal 2019;52:80–96.
[36] Pisarchik AN, Andreev AV, Kurkin SA, Stoyanov D, Badarin AA, Paunova R, Hramov AE. Topology switching during window thresholding fmri-based functional networks of patients with major depressive disorder: Consensus network approach. Chaos: An Interdiscip J Nonlinear Sci 2023;33:093122.
[37] Pitsik E, Kurkin S, Martynova O, Portnova G, Hramov AE. Hypergraph representation of multilayer brain network enhances autism spectrum disorder detection. Chaos: An Interdiscip J Nonlinear Sci 2025;35:071104.
[38] Arenas A, Díaz-Guilera A, Kurths J, Moreno Y, Zhou C. Synchronization in complex networks. Phys Rep 2008;469:93–153.
[39] Boccaletti S, Latora V, Moreno Y, Chavez M, Hwang D-U. Complex networks: Structure and dynamics. Phys Rep 2006;424:175–308.
[40] Craddock C, Benhajali Y, Chu C, Chouinard F, Evans A, Jakab A, Khundrakpam BS, Lewis JD, Li Q, Milham M, et al. The neuro bureau preprocessing initiative: open sharing of preprocessed neuroimaging data and derivatives. Front Neuroinform. 2013;7:5.
[41] Yan C, Zang Y. Dparsf: a matlab toolbox for "pipeline" data analysis of resting-state fmri. Front Syst Neurosci 2010;4:1377.
[42] Craddock RC, James GA, I.I.I. PE Holtzheimer, Hu XP, Mayberg HS. A whole brain fmri atlas generated via spatially constrained spectral clustering. Hum Brain Mapp 2012;33:1914–28.
[43] Lord L-D, Expert P, Fernandes HM, Petri G, Hartevelt TJ Van, Vaccarino F, Deco G, Turkheimer F, Kringelbach ML. Insights into brain architectures from the homological scaffolds of functional connectivity networks. Front Syst Neurosci 2016;10:85.
[44] Simon N, Friedman J, Hastie T, Tibshirani R. A sparse-group lasso. J Comput Graph Statist 2013;22:231–45.
[45] Guo H, Li Y, Xu Y, Jin Y, Xiang J, Chen J. Resting-state brain functional hyper-network construction based on elastic net and group lasso methods. Front Neuroinform. 2018;12:25.
[46] Tzourio-Mazoyer N, Landeau B, Papathanassiou D, Crivello F, Etard O, Delcroix N, Mazoyer B, Joliot M. Automated anatomical labeling of activations in spm using a macroscopic anatomical parcellation of the mni mri single-subject brain. Neuroimage 2002;15:273–89.
[47] Kipf TN, Welling M. Semi-supervised classification with graph convolutional networks. In: International conference on learning representations. 2017.
[48] Yeo BT, Krienen FM, Sepulcre J, Sabuncu MR, Lashkari D, Hollinshead M, Roffman JL, Smoller JW, Zöllei L, Polimeni JR, et al. The organization of the human cerebral cortex estimated by intrinsic functional connectivity. J Neurophysiol 2011.
[49] Menon V. Large-scale brain networks and psychopathology: a unifying triple network model. Trends Cogn Sci 2011;15:483–506.
[50] Buckner RL, Krienen FM, Castellanos A, Diaz JC, Yeo BT. The organization of the human cerebellum estimated by intrinsic functional connectivity. J Neurophysiol 2011;106:2322–45.
[51] Virtanen P, Gommers R, Oliphant TE, Haberland M, Reddy T, Cournapeau D, Burovski E, Peterson P, Weckesser W, Bright J, van der Walt SJ, Brett M, Wilson J, Millman KJ, Mayorov N, Nelson ARJ, Jones E, Kern R, Larson E, Carey CJ, Polat İ, Feng Y, Moore EW, VanderPlas J, Laxalde D, Perktold J, Cimrman R, Henriksen I, Quintero EA, Harris CR, Archibald AM, Ribeiro AH, Pedregosa F, van Mulbregt P, SciPy 10 Contributors. SciPy 1.0: Fundamental Algorithms for Scientific Computing in Python. Nature Methods 2020;17:261–72. http://dx.doi.org/10.1038/s41592-019-0686-2.
[52] Pedregosa F, Varoquaux G, Gramfort A, Michel V, Thirion B, Grisel O, Blondel M, Prettenhofer P, Weiss R, Dubourg V, Vanderplas J, Passos A, Cournapeau D, Brucher M, Perrot M, Duchesnay E. Scikit-learn: Machine learning in python. J Mach Learn Res 2011;12:2825–30.
[53] Hajij M, Zamzmi G, Papamarkou T, Miolane N, Guzmán-Sáenz A, Ramamurthy KN, Birdal T, Dey TK, Mukherjee S, Samaga SN, Livesay N, Walters R, Rosen P, Schaub MT. Topological deep learning: Going beyond graph data. 2023, arXiv:2206.00606.
[54] Han X, Li J. Leveraging unified multi-view hypergraph learning for neurodevelopmental disorders diagnosis. Front Med 2025;12:1654199.
[55] Arora M, Jain CS, Baru LB, Dadi K, et al. Hypergale: Asd classification via hypergraph gated attention with learnable hyperedges. In: 2024 international joint conference on neural networks. IJCNN, IEEE; 2024, p. 1–8.
[56] Han X, Xue R, Du S, Gao Y. Inter-intra high-order brain network for asd diagnosis via functional mris. In: International conference on medical image computing and computer-assisted intervention. Springer; 2024, p. 216–26.
[57] Hao X, An Q, Li J, Min H, Guo Y, Yu M, Qin J. Exploring high-order correlations with deep-broad learning for autism spectrum disorder diagnosis. Front Neurosci 2022;16:1046268.
[58] Uddin LQ, Supekar K, Lynch CJ, Khouzam A, Phillips J, Feinstein C, Ryali S, Menon V. Salience network–based classification and prediction of symptom severity in children with autism. JAMA Psychiatry 2013;70.
[59] Rudie JD, Brown J, Beck-Pancer D, Hernandez L, Dennis E, Thompson P, Bookheimer S, Dapretto M. Altered functional and structural brain network organization in autism. NeuroImage: Clin 2013;2:79–94.
[60] Yang C, Wang P, Tan J, Liu Q, Li X. Autism spectrum disorder diagnosis using graph attention network based on spatial-constrained sparse functional brain networks. Comput Biol Med 2021;139:104963.
[61] Chen Y, Yan J, Jiang M, Zhang T, Zhao Z, Zhao W, Zheng J, Yao D, Zhang R, Kendrick KM, et al. Adversarial learning based node-edge graph attention networks for autism spectrum disorder identification. IEEE Trans Neural Netw. Learn Syst 2022;35:7275–86.
[62] Zhang J, Guo J, Lu D, Cao Y. Asd-swnet: a novel shared-weight feature extraction and classification network for autism spectrum disorder diagnosis. Sci Rep 2024;14:13696.
[63] Wang W, Xiao L, Qu G, Calhoun VD, Wang Y-P, Sun X. Multiview hyperedge-aware hypergraph embedding learning for multisite, multiatlas fmri based functional connectivity network analysis. Med Image Anal 2024;94:103144.
[64] Hong S-J, de Wael R Vos, Bethlehem RA, Lariviere S, Paquola C, Valk SL, Milham MP, Martino A Di, Margulies DS, Smallwood J, et al. Atypical functional connectome hierarchy in autism. Nat Commun 2019;10:1022.
[65] Zhang K, Li Q, Yu S. Mvho-ib: Multi-view higher-order information bottleneck for brain disorder diagnosis. In: International conference on medical image computing and computer-assisted intervention. Springer; 2025, p. 407–17.

[66] Khan AJ, Nair A, Keown CL, Datko MC, Lincoln AJ, Müller R-A. Cerebro-cerebellar resting-state functional connectivity in children and adolescents with autism spectrum disorder. Biol Psychiatry 2015;78:625–34.
[67] Stoodley CJ, D'Mello AM, Ellegood J, Jakkamsetti V, Liu P, Nebel MB, Gibson JM, Kelly E, Meng F, Cano CA, et al. Altered cerebellar connectivity in autism and cerebellar-mediated rescue of autism-related behaviors in mice. Nature Neurosci 2017;20:1744–51.
[68] Hull JV, Dokovna LB, Jacokes ZJ, Torgerson CM, Irimia A, Horn JD Van. Resting-state functional connectivity in autism spectrum disorders: a review. Front Psychiatry 2017;7:205.
[69] Heinsfeld AS, Franco AR, Craddock RC, Buchweitz A, Meneguzzi F. Identification of autism spectrum disorder using deep learning and the abide dataset. NeuroImage: Clin 2018;17:16–23.
[70] Zhao F, Chen Z, Rekik I, Lee S-W, Shen D. Diagnosis of autism spectrum disorder using central-moment features from low-and high-order dynamic resting-state functional connectivity networks. Front Neurosci 2020;14:258.